ACS APPLIED ENERGY MATERIALS

www.acsaem.org Article

Anomalous Lattice Thermal Conductivity in Rocksalt IIA–VIA Compounds

S. C. Rakesh Roshan,* N. Yedukondalu,* Rajmohan Muthaiah, Kunduru Lavanya, Pazhedath Anees, Rajaboina Rakesh Kumar, Tumu Venkatappa Rao, Lars Ehm, and John B. Parise

Cite This: *ACS Appl. Energy Mater.* 2022, 5, 882–896 Read Online

ACCESS | Metrics & More | Article Recommendations | Supporting Information

ABSTRACT: Materials with an intrinsic (ultra)low lattice thermal conductivity (k_L) are critically important for the development of efficient energy conversion devices. In the present work, we have investigated microscopic origins of low k_L behavior in BaO, BaS, and MgTe by exploring lattice dynamics and phonon transport of 16 isostructural MX (M = Mg, Ca, Sr, and Ba and X = O, S, Se, and Te) compounds in the rocksalt (NaCl)-type structure. Anomalous trends are observed for k_L in MX (M = Mg, Ca, Sr, and Ba and X = O, S, Se, and Te) compounds except for the MgX (X = O, S, Se, and Te) series in contrast to the expected trend from their atomic mass. The underlying mechanisms for such low k_L behavior in large mismatch atomic mass systems, namely, BaO, BaS, and MgTe, are thoroughly analyzed. We propose the following factors that might be responsible for low k_L behavior in these materials: (1) high mass contrast provides a phonon gap between the acoustic and optic branches; (2) softening of transverse acoustic (TA) phonon modes due to the presence of heavy element; (3) low-lying optic (LLO) phonon modes fall into the acoustic mode region and are responsible for softening of the acoustic phonon modes or enhancing the overlap between LLO (TO) and longitudinal acoustic (LA) phonon modes, thereby increasing scattering rates; (4) shorter phonon lifetimes; and (5) a relatively high density (ρ) and a large Grüneisen parameter (γ) leads to strong anharmonicity. Moreover, tensile strain causes a further reduction in k_L for BaO, BaS, and MgTe through phonon softening and near ferroelectric instability. Our comprehensive study on 16 binary MX (M = Mg, Ca, Sr, and Ba and X = O, S, Se, and Te) compounds provides a pathway for designing (ultra)low k_L materials through phonon engineering even with simple crystal systems.

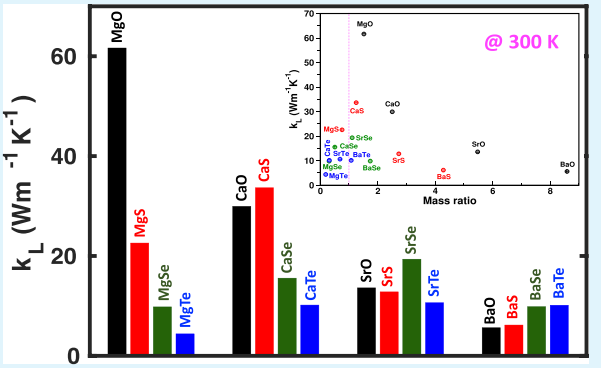

KEYWORDS: *finite temperature lattice dynamics, lattice thermal conductivity, rocksalt-type, mass contrast, phonon transport, temperature-dependent effective potential (TDEP), first-principles calculations, molecular dynamics simulations*

Downloaded via NATL INST OF TECH WARANGAL on September 15, 2025 at 09:51:16 (UTC).
See https://pubs.acs.org/sharingguidelines for options on how to legitimately share published articles.

INTRODUCTION

Materials with low lattice thermal conductivity (k_L) have gained tremendous interest because of their potential applications in thermoelectrics,[1,2] thermal barrier coatings,[3] thermal insulation,[4] and thermal energy management. Extensive efforts have been put forward by researchers in this direction to develop suitable materials for energy conversion applications during the past decade. Binary alkaline-earth chalcogenides, MX (M = Mg, Ca, Sr, and Ba and X = O, S, Se, and Te) are simple binary systems and are receiving considerable attention because of their possible applications in thermoelectrics.[5−7] Bulk MX and their 2D counterparts,[5−8] p-type PbTe and MTe nanocrystals,[9] CaTe-SnTe,[10] heavily doped SrTe with PbTe,[11,12] and BaTe-PbTe,[13] are found to have excellent thermoelectric figure of merit (zT) in the range of 0.5−1.32.[7,14] In general, the conversion efficiency is characterized by a dimensionless quantity i.e., $zT = S\sigma^2T/k$, where $k = k_e + k_L$; S, σ, T are the Seebeck coefficient, electrical conductivity, and absolute temperature, and k_e & k_L are the electronic and lattice thermal conductivities, respectively. The complex interdependence among these S, σ, and k parameters makes it challenging to discover the high zT materials. Therefore, materials with an intrinsic ultralow k (especially k_L) provide a pathway for discovering high zT materials without degrading its charge transport.

The MX (M = Mg, Ca, Sr, and Ba and X = O, S, Se, and Te) compounds are extensively studied from the theoretical perspective, which mainly focused on exploring the elastic,[15,16] lattice dynamics,[17−20] thermodynamic,[21,22] and thermoelectric

Received: October 21, 2021
Accepted: December 15, 2021
Published: December 29, 2021

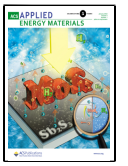

© 2021 American Chemical Society

https://doi.org/10.1021/acsaem.1c03310
ACS Appl. Energy Mater. 2022, 5, 882–896

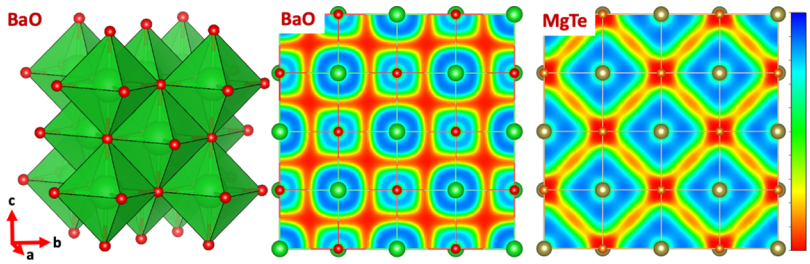

Figure 1. Crystal structure of BaO and electron localization function (ELF) of BaO and MgTe along the (001) plane. Light green (#1EEF2C), red (#FE0300), thick orange (#FB7B15) and light brown (#ADA251) color balls represent Ba, O, Mg and Te atoms, respectively. The values in parenthesis are hexadecimal color codes.

properties[5−7] at ambient and/or high-pressure conditions. However, very limited studies have been dedicated toward understanding the phonon transport in MgSe,[23] MgTe,[24] CaX (X = O, S, Se, and Te)[25] and MTe (M = Mg, Ca, Sr, Ba, and Pb)[26] compounds. Therefore, a detailed and comparative study on phonon transport of MX (M = Mg, Ca, Sr, and Ba and X = O, S, Se, and Te) compounds provide insights to achieve (ultra)low k_L materials through phonon engineering, which is essential for the discovery of high zT materials. In the present work, we shed more light on understanding lattice dynamics, phonon transport, and mechanical properties of 16 MX (M = Mg, Ca, Sr, and Ba and X = O, S, Se, and Te) compounds at ambient conditions. Interestingly, we observe anomalous trends in k_L for CaX (CaS > CaO > CaSe > CaTe), SrX (SrSe > SrO > SrS > SrTe), and BaX (BaTe > BaSe > BaS > BaO) series. Especially, the observed anomalous[27] trend in BaX (partly in SrX and CaX[25]) series is in contrast to the expected trend from their atomic mass. Overall, among 16 compounds, we found BaO, BaS, and MgTe to exhibit low k_L behavior over the studied temperature range of 300−800 K despite their low atomic mass in the rocksalt NaCl-type (B1) structure. The underlying mechanisms for such abnormal trends and low k_L behavior are extensively discussed through the computed lattice dynamics, phonon lifetimes, scattering rates, phonon group velocities at 300 K, and mechanical properties. We have also investigated the effect of tensile strain on the lattice dynamics and the phonon transport properties of BaO, BaS, and MgTe compounds and discussed it in detail.

The rest of the paper is organized as follows: In the next section, we briefly describe the computational details, the methodology, various parameters used to perform the computation, and the crystal structure. Results concerning anharmonic lattice dynamics, lattice thermal conductivity, and mechanical properties of the 16 MX (M = Mg, Ca, Sr, and Ba and X = O, S, Se, and Te) compounds are discussed. Finally, we propose important observations that will be helpful to achieve (ultra)low k_L in general and summarized major outcomes of the present study.

COMPUTATIONAL DETAILS, METHODOLOGY, AND CRYSTAL STRUCTURE

All the first-principles calculations have been performed using the *Vienna Ab initio Simulation Package* (*VASP*)[28] for MX (M = Mg, Ca, Sr, and Ba and X = O, S, Se, and Te) compounds. The exchange-correlation was treated with the PBEsol functional and the electron−ion interactions with the pseudopotential-based projected augmented wave (PAW) approach. We have considered 10 and 6 valence electrons for alkaline-earth metals (Mg, Ca, Sr, and Ba) and chalcogens (O, S, Se, and Te) as plane wave basis orbitals, respectively. A plane wave cutoff energy of 520 eV was used for plane wave basis set expansion and a spacing of $2\pi \times 0.024$ Å^{-1} for k-mesh in the irreducible Brillouin zone. Because MX (M = Mg, Ca, Sr, and Ba and X = O, S, Se, and Te) compounds are polar semiconductors, Born effective charges and dielectric constants are calculated using density functional perturbation theory to capture dipole−dipole interactions.

Lattice dynamics and thermal conductivity of MX (M = Mg, Ca, Sr, and Ba and X = O, S, Se, and Te) compounds are calculated by considering harmonic (second) and anharmonic (third) interatomic force constants (IFCs) using the temperature-dependent effective potential (TDEP)[29−31] method. In the present work, we have considered the expansion of interatomic force constants (IFCs) up to third order and the corresponding model Hamiltonian is given as follows:

$$H = U_0 + \sum_i \frac{p_i^2}{2m_i} + \frac{1}{2!}\sum_{ij}\sum_{\alpha\beta} \Phi_{ij}^{\alpha\beta} u_i^{\alpha} u_j^{\beta} + \frac{1}{3!}\sum_{ijk}\sum_{\alpha\beta\gamma} \psi_{ijk}^{\alpha\beta\gamma} u_i^{\alpha} u_j^{\beta} u_k^{\gamma} \quad (1)$$

where p_i and u_i are the momentum and displacement of atom i, respectively. $\Phi_{ij}^{\alpha\beta}$ and $\psi_{ijk}^{\alpha\beta\gamma}$ are second- and third-order force constant matrices, respectively. To compute these harmonic (second) and anharmonic (third) interatomic force constants (IFCs), we have performed ab initio molecular dynamics (AIMD) simulations as implemented in the *VASP* at 300 K. The AIMD calculations were run for 5000 MD steps with time-step of 1 fs (i.e., 5 ps) with 128 atoms (4 × 4 × 4) supercell for all the investigated compounds. For second- and third-order IFCs, interactions up to ninth nearest neighbors were included to ensure the convergence of calculated lattice dynamics and phonon transport properties. The temperature was controlled with a Nosé−Hoover thermostat. The lattice thermal conductivity is calculated by iteratively solving the full Boltzmann transport equation (BTE), including three-phonon and isotope scatterings from the natural distribution on a 25 × 25 × 25 q-point grid.

The thermal conductivity tensor is given by

$$k^{\alpha\beta} = \frac{1}{(2\pi)^3}\sum_s \int dq C_\lambda v_{\lambda\alpha} v_{\lambda\beta} \tau_{\lambda\beta} \quad (2)$$

where C_λ is the contribution per mode $\lambda = (s, q)$ to specific heat, α and β are Cartesian components, and v_β and τ_β are phonon velocity and scattering time, respectively.

The scattering rates are calculated from a full inelastic phonon Boltzmann equation which is given by

https://doi.org/10.1021/acsaem.1c03310
ACS Appl. Energy Mater. 2022, 5, 882−896

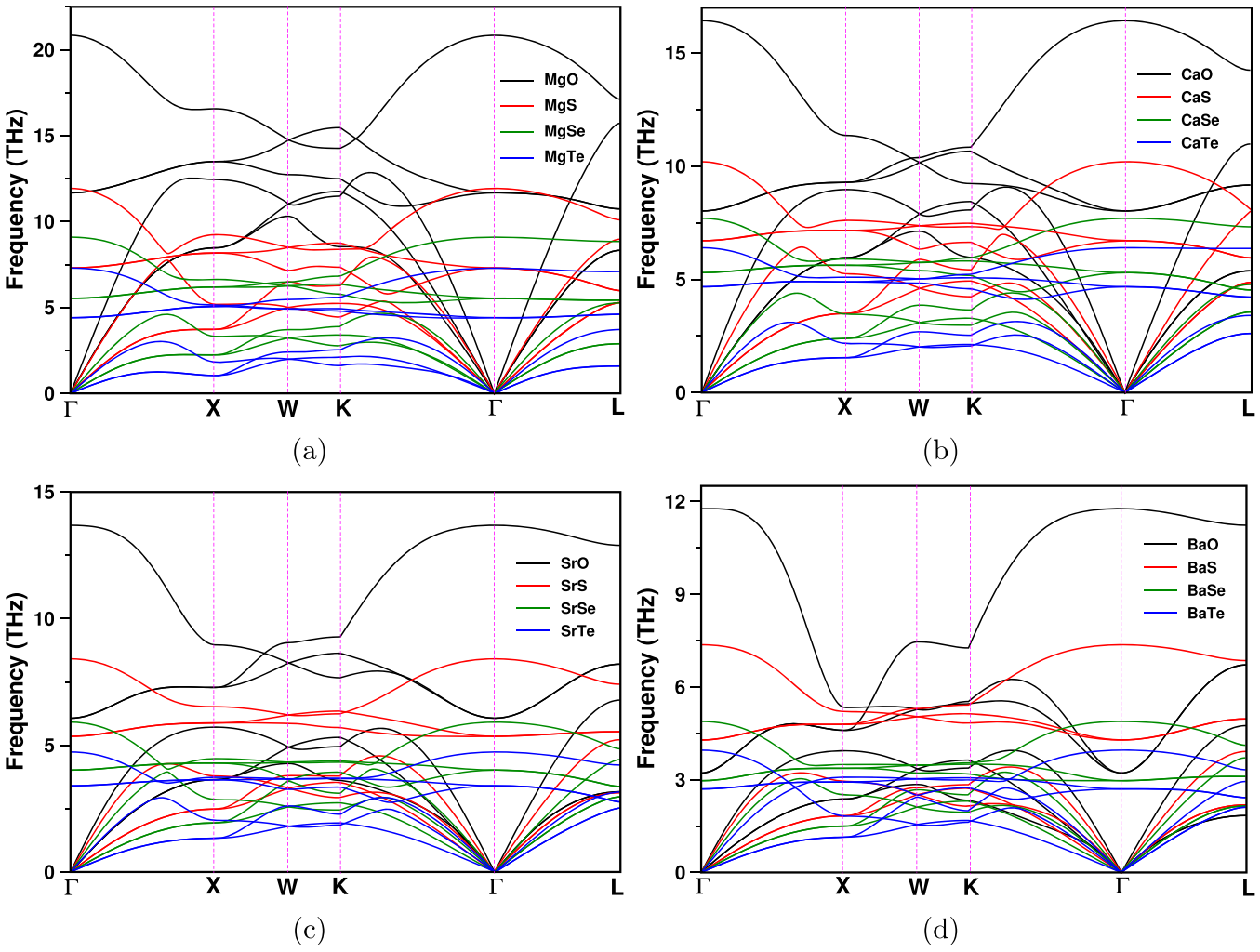

Figure 2. Calculated room-temperature phonon dispersion curves of (a) MgX, (b) CaX, (c) SrX, and (d) BaX compounds at the PBEsol equilibrium volume, where X = O, S, Se, and Te. Phonon softening is observed with increasing atomic mass of both alkaline-earth (Mg, Ca, Sr, Ba) and chalcogen (O, S, Se, Te) atoms.

$$k_B T v_\lambda \nabla T \frac{\partial n_{0\lambda}}{\partial T} = \sum_{\lambda'\lambda''} \left[P^{+}_{\lambda\lambda'\lambda''}(\Psi_{\lambda''} - \Psi_{\lambda'} - \Psi_{\lambda}) + \frac{1}{2} P^{-}_{\lambda\lambda'\lambda''}(\Psi_{\lambda''} + \Psi_{\lambda'} - \Psi_{\lambda}) \right] \quad (3)$$

The left-hand side represents the phonon diffusion induced by the thermal gradient ∇T and $n_{0\lambda}$ is the equilibrium phonon distribution function. The right-hand side corresponds to the collision term for three-phonon interactions. v_λ is the phonon velocity in mode λ, $P^{+}_{\lambda\lambda'\lambda''}$, and $P^{-}_{\lambda\lambda'\lambda''}$ are three phonon scattering rates for absorption ($\lambda + \lambda' \rightarrow \lambda''$) and emission ($\lambda \rightarrow \lambda' + \lambda''$) processes, respectively.

Binary alkaline-earth chalcogenides, MX (M = Mg, Ca, Sr, and Ba and X = O, S, Se, and Te) compounds except MgSe and MgTe crystallize in the face-centered cubic (FCC) rocksalt NaCl (B1)-type structure (see Figure 1) having space group $Fm\bar{3}m$ with $Z = 4$ formula units (f.u.) per unit cell at ambient conditions.[32−38] MgSe and MgTe exhibit rich polymorphism and they crystallize in rocksalt (B1), zincblende (B3), wurtzite (B4), and NiAs (B8)-type structures. The X-ray diffraction measurements reveal that MgTe crystallizes in B3[39] and B8[40] structures at ambient conditions. First-principles calculations disclose that B3[41] phase for MgSe and both B3[41] and B8[42−44] for MgTe are thermodynamically stable structures at ambient conditions. Moreover, rocksalt-type B1 structure is dynamically stable (metastable) for both MgSe and MgTe compounds. Therefore, in the present work, we have considered B1 structure for all the MX (M = Mg, Ca, Sr, and Ba and X = O, S, Se, and Te) compounds, which allow us to directly compare the calculated properties among these 16 compounds under investigation. Table S1 presents the calculated ground-state equilibrium lattice constant for MX (M = Mg, Ca, Sr, and Ba and X = O, S, Se, and Te) compounds in comparison with reported X-ray diffraction measurements[32−37,45−47] and previous first-principles calculations[5,7,41,48−51] and there is a good agreement among them. In addition, we also calculated the electron localization function (ELF) for BaO and MgTe compounds. As shown in Figure 1, the metal cations (Mg^{2+}, Ba^{2+}) donate the electrons, whereas anions (O^{2-}, Te^{2-}) gain the electrons, indicating complete transfer of charge and resulting in strong ionic bonding that is consistent with the fact that a large electronegativity (on the pauling scale) difference (2.55 for BaO) between Ba (0.89) and O (3.44) results in strong ionic character. The low electronegativity difference (0.79 for MgTe) between Mg (1.31) and Te (2.10) atoms suggest a polar covalent bonding along with ionic bonding in

https://doi.org/10.1021/acsaem.1c03310
ACS Appl. Energy Mater. 2022, 5, 882−896

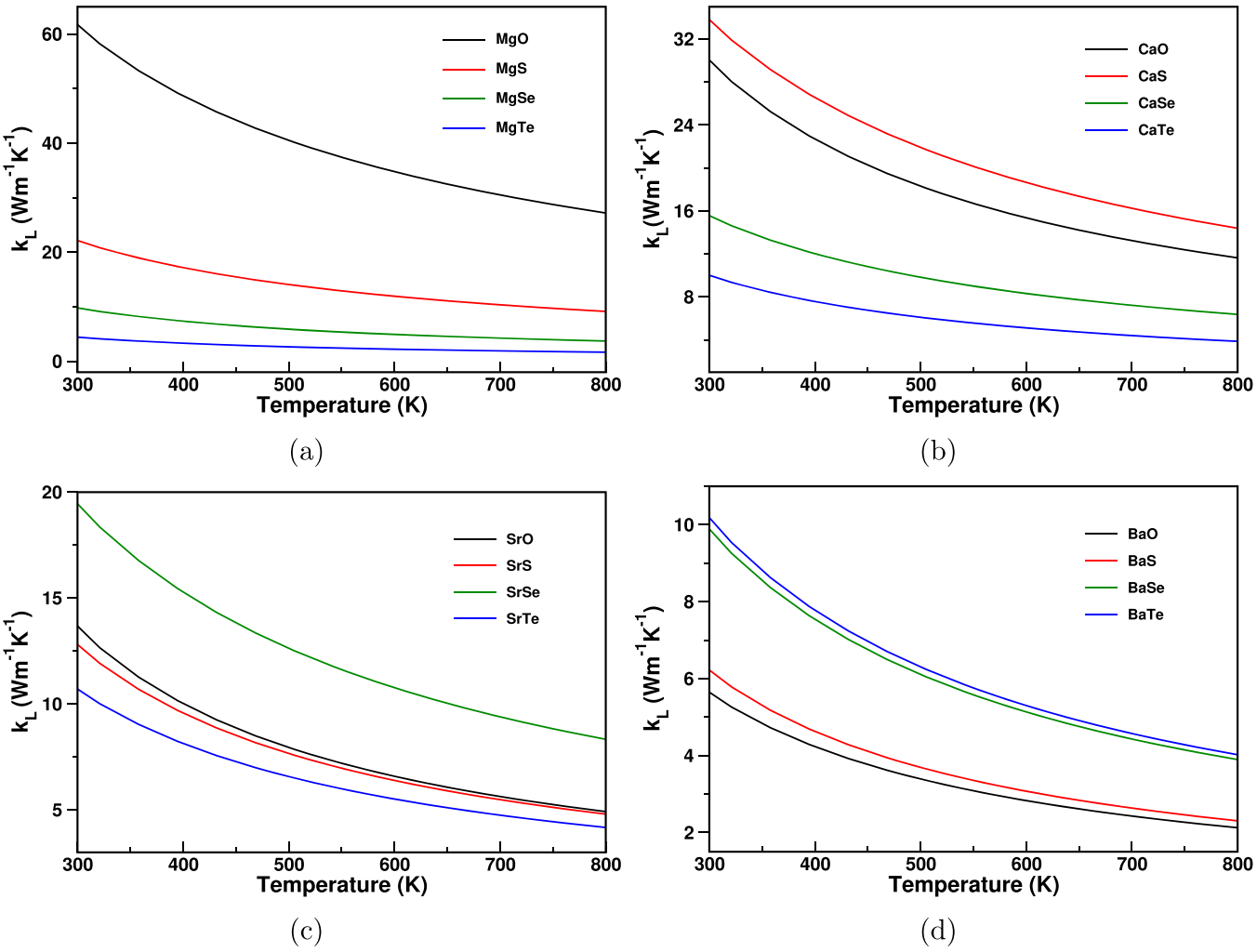

Figure 3. Calculated lattice thermal conductivity (k_L) of (a) MgX, (b) CaX, (c) SrX, and (d) BaX compounds as a function of temperature, where X = O, S, Se, and Te at the PBEsol equilibrium volume. Anomalous trends are predicted for k_L partly in CaX (CaS > CaO > CaSe > CaTe), SrX (SrSe > SrO > SrS > SrTe) and a completely opposite trend for BaX (BaTe > BaSe > BaS > BaO) compounds in contrast to the trends expected from their atomic mass.

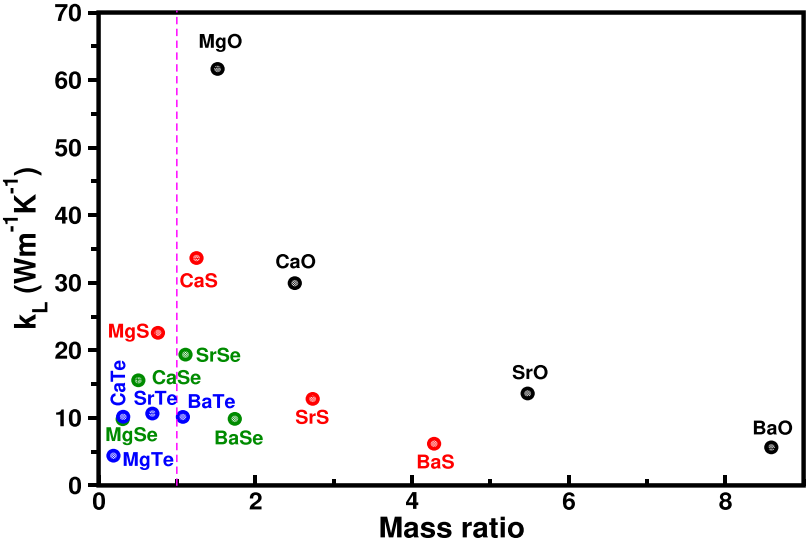

Figure 4. Calculated lattice thermal conductivity (k_L) at 300 K as a function of mass ratio for MX (M = Mg, Ca, Sr, and Ba and X = O, S, Se, and Te) compounds. The vertical line corresponds to mass ratio equal to unity, where metal and nonmetal atoms have equal atomic masses.

https://doi.org/10.1021/acsaem.1c03310
ACS Appl. Energy Mater. 2022, 5, 882−896

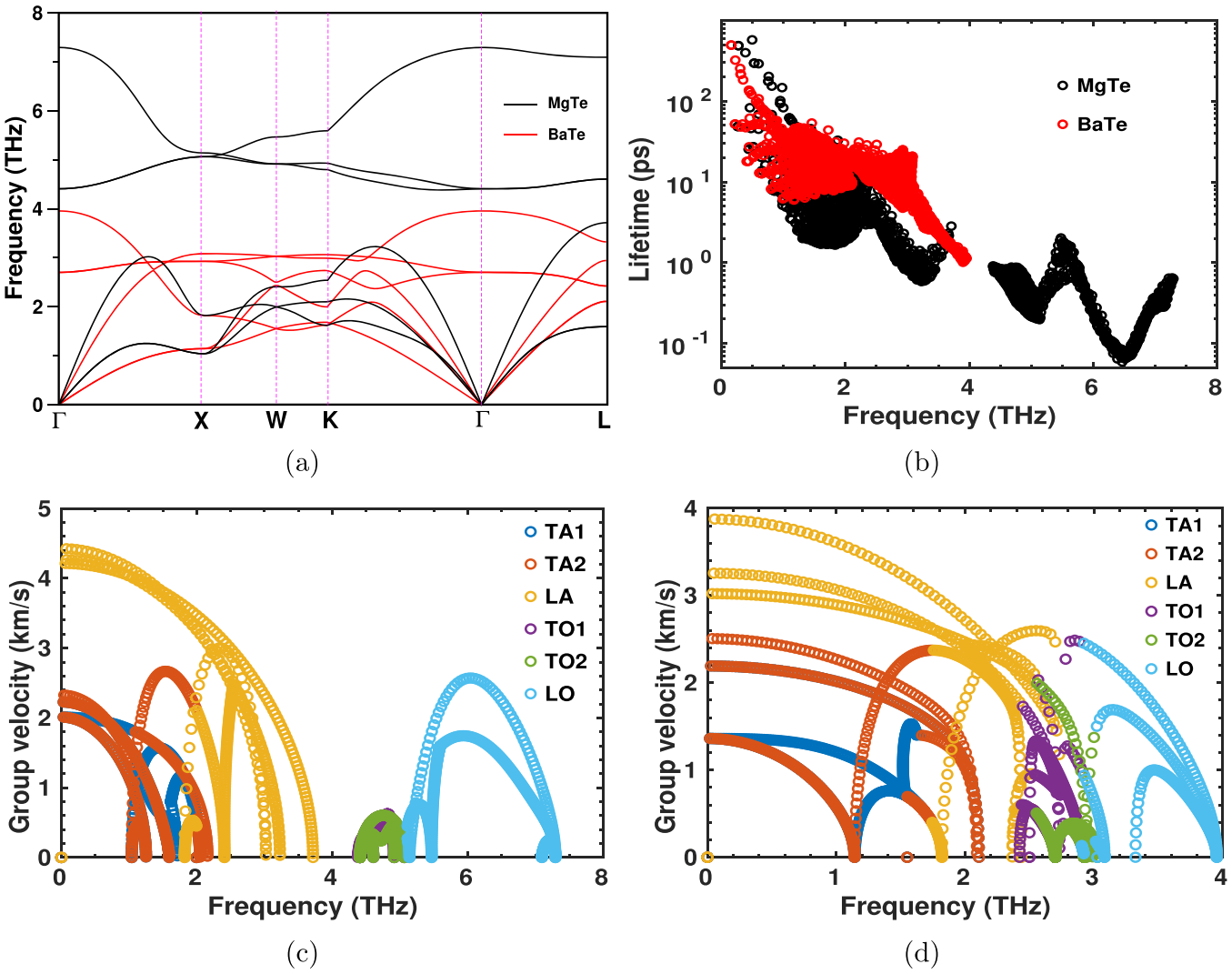

Figure 5. Calculated (a) phonon dispersion curves, (b) phonon lifetimes of MgTe and BaTe as a function of frequency, (c) group velocity as a function of frequency for MgTe, and (d) group velocity as a function of frequency for BaTe.

Table 1. Calculated Lattice Thermal Conductivity (k_L, in W m^{-1} K^{-1}) at 300 K for 16 MX Compounds

	this work		others				
compd	k_L[a]	k_L^E[b]	expt.	k_{3ph}^{HA}	k_{3ph}^{SCPH}	$k_{3,4ph}^{SCPH}$	others
MgO	61.65	61.65	52[c]	52.1[d]	58.7[d]	50.1[d]	
MgS	22.59	18.74					
MgSe	9.8	7.55					
MgTe	4.45	4.45					3.5[e], 3[f]
CaO	29.94	24.77	30[c]	21.3[d]	25.1[d]	22.2[d]	
CaS	33.66	28.39					
CaSe	15.56	13.21					
CaTe	10.17	8.33					3.1[e], 8.5[f]
SrO	13.61	11.65	10[c]	9.0[d]	11.0[d]	9.9[d]	
SrS	12.81	11.60					
SrSe	19.36	15.8					
SrTe	10.64	9.66					2.5[e], 10.5[f]
BaO	5.63	6.76	3[c]	2.8[d]	4.4[d]	3.3[d]	
BaS	6.17	6.28					
BaSe	9.85	10.06					
BaTe	10.14	9.84					1.9[e], 10.2[f]

[a] k_L: calculated at the PBEsol equilibrium lattice constant [b] k_L^E: calculated at the experimental lattice constant [c] Ref 69. [d] Ref 70. [e] Ref 54. [f] Ref 26.

https://doi.org/10.1021/acsaem.1c03310
ACS Appl. Energy Mater. 2022, 5, 882−896

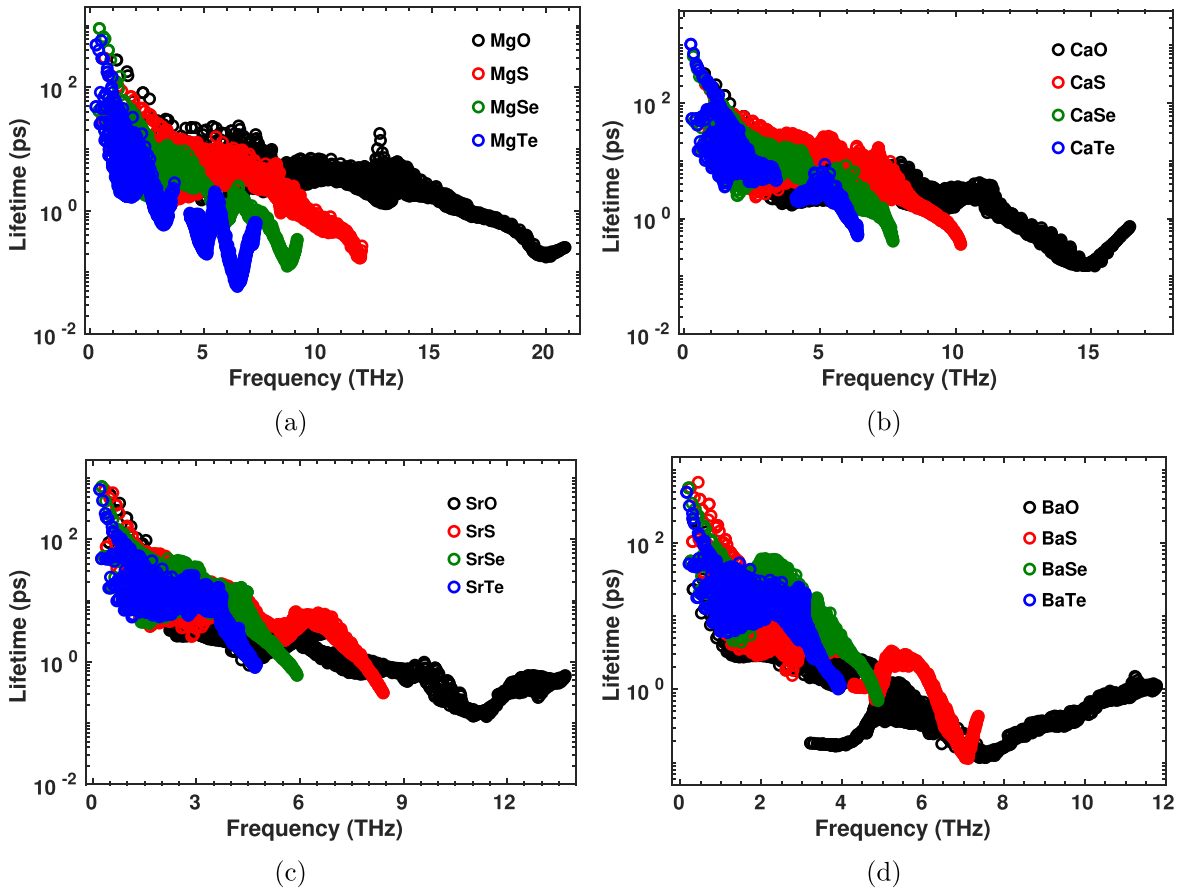

Figure 6. Calculated phonon lifetimes of (a) MgX, (b) CaX, (c) SrX, and (d) BaX compounds as a function of frequency, where X = O, S, Se, and Te.

MgTe. The distinct nature of chemical bonding strongly influences k_L of these materials.

RESULTS AND DISCUSSION

Anharmonic Lattice Dynamics and Thermal Conductivity. Exploring lattice dynamics including anharmonic effects is crucial for understanding phonon transport in materials. As a first step, we have computed phonon dispersion curves (Figure 2) of MX (M = Mg, Ca, Sr, and Ba and X = O, S, Se, and Te) compounds at 300 K and thoroughly analyzed them. As shown in Figure 2, no imaginary frequencies are found along high symmetry directions of the Brillouin zone, indicating that all the investigated materials are dynamically stable. MX (M = Mg, Ca, Sr, and Ba and X = O, S, Se, and Te) materials consist of two atoms per primitive cell resulting in ($3N$; N = number of atoms per primitive cell) six vibrational modes, of which three are acoustic and three are optic modes. Dipole−dipole interactions are crucial for polar materials to describe phonon spectra correctly. These interactions are incorporated into a dynamic matrix through calculated Born effective charges (see Table S2) and high-frequency dielectric constants, which in turn produces a splitting between the longitudinal optic (LO) and transverse optic (TO) phonon modes (Figure 2). Because of this LO-TO splitting, the three phonon optic modes split into two degenerate TO (ω_{TO}) and one LO (ω_{LO}) modes along the Γ-direction. Large LO-TO splitting is observed in particular for MO (M = Mg, Ca, Sr, Ba) compounds and it increases from MgO < CaO < SrO < BaO, and it decreases from MO > MS > MSe > MTe (M = Mg, Ca, Sr, and Ba) compounds (see Figure 2 and Tables S2 and S3). The MX (M = Mg, Ca, Sr, and Ba and X = O, S, Se, and Te) compounds exhibit similar phonon band features and showed a significant phonon softening with increasing atomic mass from Mg → Ca → Sr → Ba and O → S → Se → Te, and these features are consistent with previous first-principles lattice dynamics calculations.[5−7,26]

We then calculated lattice thermal conductivity (k_L) as a function of temperature (300−800 K) and the same is presented in Figure 3. The obtained k_L values decrease with temperature for all 16 compounds under investigation because of increasing anharmonicity with temperature. Usually, materials with same crystal structure that consist of heavy elements possess low k_L compared to the ones with light elements because of their high atomic mass. As expected, k_L decreases with increasing atomic mass of anion i.e., from MgO → MgS → MgSe → MgTe in MgX compounds, whereas k_L shows anomalous trends for the CaX (CaS > CaO > CaSe > CaTe), SrX (SrSe > SrO > SrS > SrTe), and BaX (BaTe > BaSe > BaS > BaO) series of compounds. Especially, BaX series shows an opposite trend for k_L in contrary to the expected trend from their atomic mass. However, the above trends are slightly altered when k_L is computed at the experimental lattice constant for SrX (SrSe > SrO ≥ SrS > SrTe) and BaX (BaSe ≥ BaTe > BaO > BaS) compounds but the overall trends remain more or less similar in both the cases (see Figures 3 and Figures S1 and S2). To get insights on the observed anomalous trends, we have plotted the obtained k_L values at 300 K as a function of mass ratio (i.e., the ratio of the

https://doi.org/10.1021/acsaem.1c03310
ACS Appl. Energy Mater. 2022, 5, 882−896

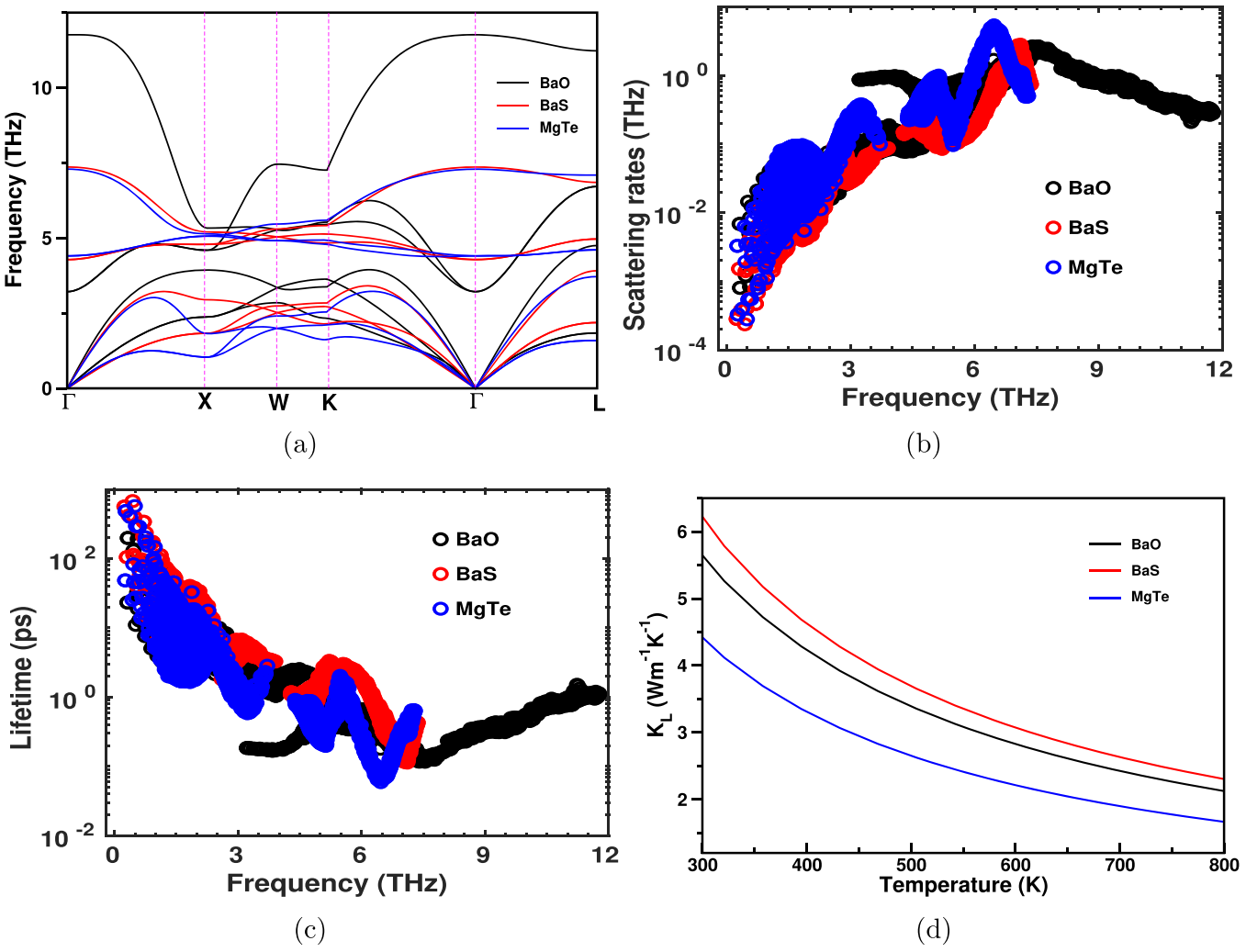

Figure 7. Calculated (a) phonon dispersion curves, (b) phonon scattering rates, (c) phonon lifetime, and (d) lattice thermal conductivity (k_L) of BaO, BaS, and MgTe compounds at PBEsol equilibrium volume. The obtained k_L values decrease in the following order: BaS > BaO > MgTe.

atomic mass of a metal atom to the atomic mass of a nonmetal atom) as depicted in Figure 4. Materials with high mass contrast, i.e., either low or high mass ratios, exhibit low k_L values. For instance, MgTe, BaS, and BaO have relatively low k_L values of 4.45, 6.17, and 5.63 W m^{-1} K^{-1} with mass ratios of 0.19, 4.3, and 8.6, respectively, compared to those with mass ratios close to unity, which are having higher k_L values. For example, BaTe has the mass ratio of 1.1 with a k_L value of 10.14 W m^{-1} K^{-1}, which is higher than the high mass contrast systems, namely, BaO and MgTe. Further, to understand why high mass contrast materials have relatively low k_L values[52] over the materials with mass ratio close to unity, we have considered MgTe and BaTe compounds for the case study. As shown in Figure 5a, MgTe has a phonon gap between acoustic and optic phonon branches and these phonon branches span in the frequency range of ∼0−8 THz, whereas BaTe has no phonon gap in the whole frequency range of ∼0−4 THz because of the mass ratio close to unity (1.1). According to slack theory,[53] if the gap between acoustic and optic phonon branches is quite small and the optic phonon velocity is large, then optic phonons also carry heat in crystalline materials. Therefore, in BaTe, the optic phonons also contribute for the heat conduction (see Figure 5d), whereas in MgTe, the phonon gap with low TO optic phonon velocities might be an unfavorable situation for the phonon transport (see Figure 5c). Moreover, MgTe has shorter phonon lifetimes over BaTe in the frequency range of ∼1−4 THz (see Figure 5b). Therefore, low phonon propagation and shorter phonon lifetimes of MgTe result in low k_L over BaTe. This explanation is valid for anomalous trends observed for other compounds as well (see Figure S3 for CaO and CaS). This clearly demonstrates that when designing low kappa materials with a combination of heavy and light elements to have high mass contrast that produce a finite phonon gap between acoustic-optic branches, which is critical to achieve (ultra)low k_L behavior.

We observed phonon softening from phonon dispersion curves (see Figures 2 and 5a) in compounds with high mass contrast. As shown in Figure 2c, d, low-lying TO modes of MO (M = Ca, Sr, and Ba), SrS, and BaS compounds fall into the acoustic mode region in general and in particular for BaO[7] and SrO[6] compounds (see Figure 2). In addition, BaO shows an extra phonon softening of transverse acoustic modes near L point despite its low atomic mass compared to the rest of BaX (X = S, Se, and Te) compounds. Among the 16 systems under investigation, interestingly, three compounds, namely, BaO, BaS, and MgTe with high mass contrast exhibit low k_L i.e., below ∼6 W m^{-1} K^{-1} at 300 K. Moreover, MgTe exhibits phonon softening of the transverse acoustic phonon modes

https://doi.org/10.1021/acsaem.1c03310
ACS Appl. Energy Mater. 2022, 5, 882−896

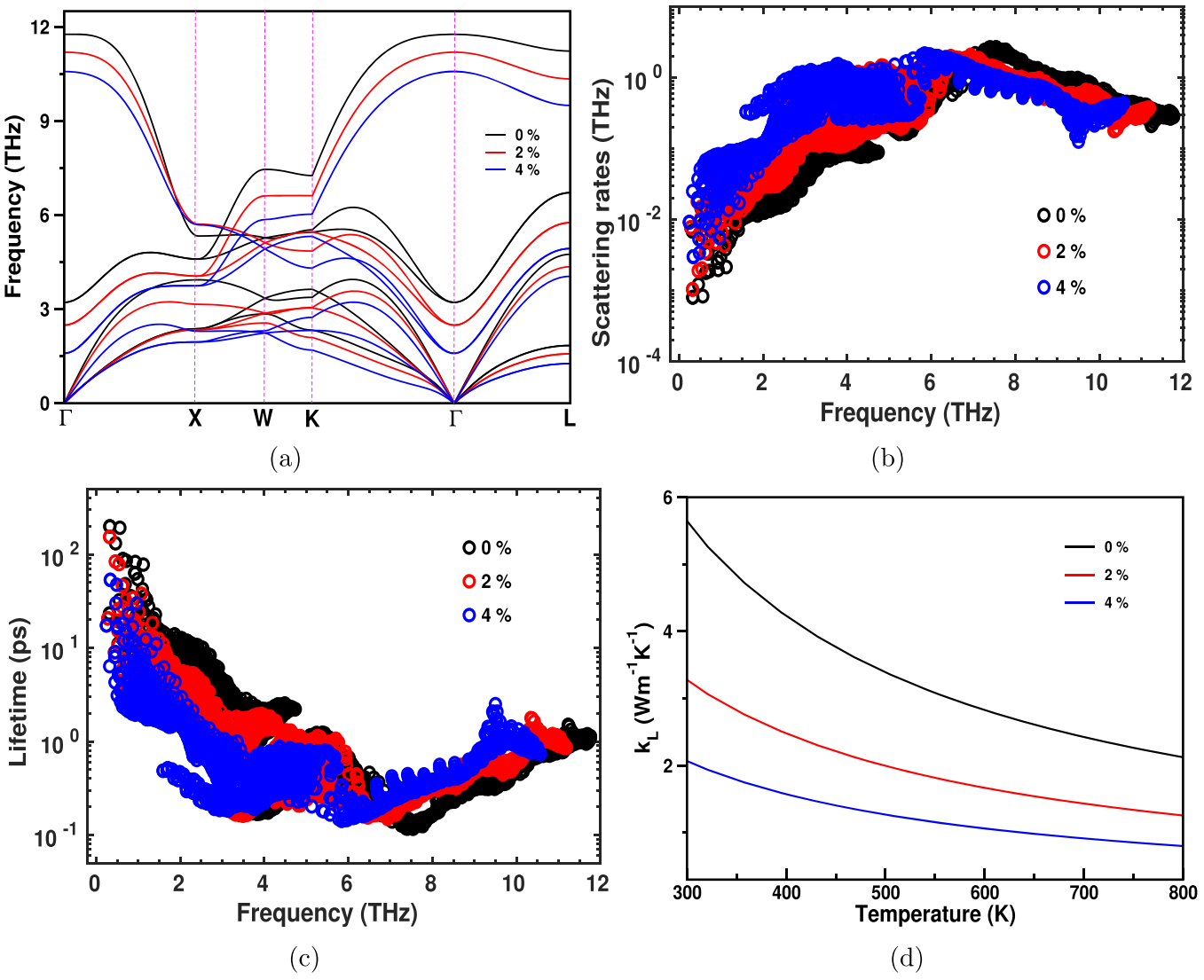

Figure 8. Calculated tensile-strain-dependent (a) phonon dispersion curves, (b) phonon scattering rates, (c) phonon lifetimes, and (d) lattice thermal conductivity (k_L) values of BaO.

near the X and L points, although it has low atomic mass compared to BaTe (see Figure 5a). This trend is consistent with the previous compressive sensing lattice dynamics (CSLD) study[26] but in contrast to the phenomenological Debye−Callaway model study[54] on the lattice thermal transport of MTe (M = Mg, Sr, Ba, and Pb) compounds. In addition, the k_L values are severely underestimated using the Debye-Callaway model (see Table 1). So far, we observed four important aspects that significantly influence the k_L behavior in BaO, BaS, and MgTe compounds: (1) high mass contrast between metal and nonmetal atoms (see Figure 4), (2) low-lying TO phonon modes fall into the acoustic mode region for BaO and BaS (see Figure 2d), (3) soft transverse acoustic (TA) phonon modes of MgTe despite its low atomic mass over BaTe (see Figure 5a), and (4) phonon lifetimes for MgTe and BaTe (see Figure 5b). Especially, the later one plays a pivotal role in determining trends in k_L, and the same is discussed in detail in the section below.

To further explore the underlying mechanisms that are responsible for the observed anomalous behavior of k_L in MgTe, CaX (X = O and S), SrX (X = O, S, and Se), and BaX (X = O, S, Se, and Te) compounds (see Figure 3 and Figure S1 and S2), we have calculated phonon mean free paths (MFPs), phonon lifetimes, group velocities, and scattering rates. The calculated phonon MFPs as a function of frequency are presented in Figure S4. For all the MX compounds, a large portion of the phonon MFPs fall above the minimum interatomic distance or so-called Ioffe−Regel limit. Therefore, the phonon Boltzmann transport theory is good enough to describe thermal transport in MX compounds. In crystalline materials, the heat transport can be understood as the propagation of phonons and their scatterings among themselves. Because $k_L \propto \tau(\omega)$ and $v(\omega)$, materials with low $\tau(\omega)$ and $v(\omega)$ are expected to have low k_L.

As illustrated in Figure 6, phonon lifetime decreases from MgO > MgS > MgSe > MgTe over the entire frequency range, and the same trend is followed for k_L in MgX. However, CaO has relatively shorter phonon lifetimes than CaS in the frequency range of ∼2−8 THz (see Figure 6b), which might be a reason for the low k_L of CaO and results in the anomalous trend (CaS > CaO > CaSe > CaTe) for k_L in the CaX series. This trend is consistent with the previous lattice thermal conductivity study[25] on CaX (X = O, S, Se, and Te) compounds using ShengBTE. SrSe and SrO possess relatively

https://doi.org/10.1021/acsaem.1c03310
ACS Appl. Energy Mater. 2022, 5, 882−896

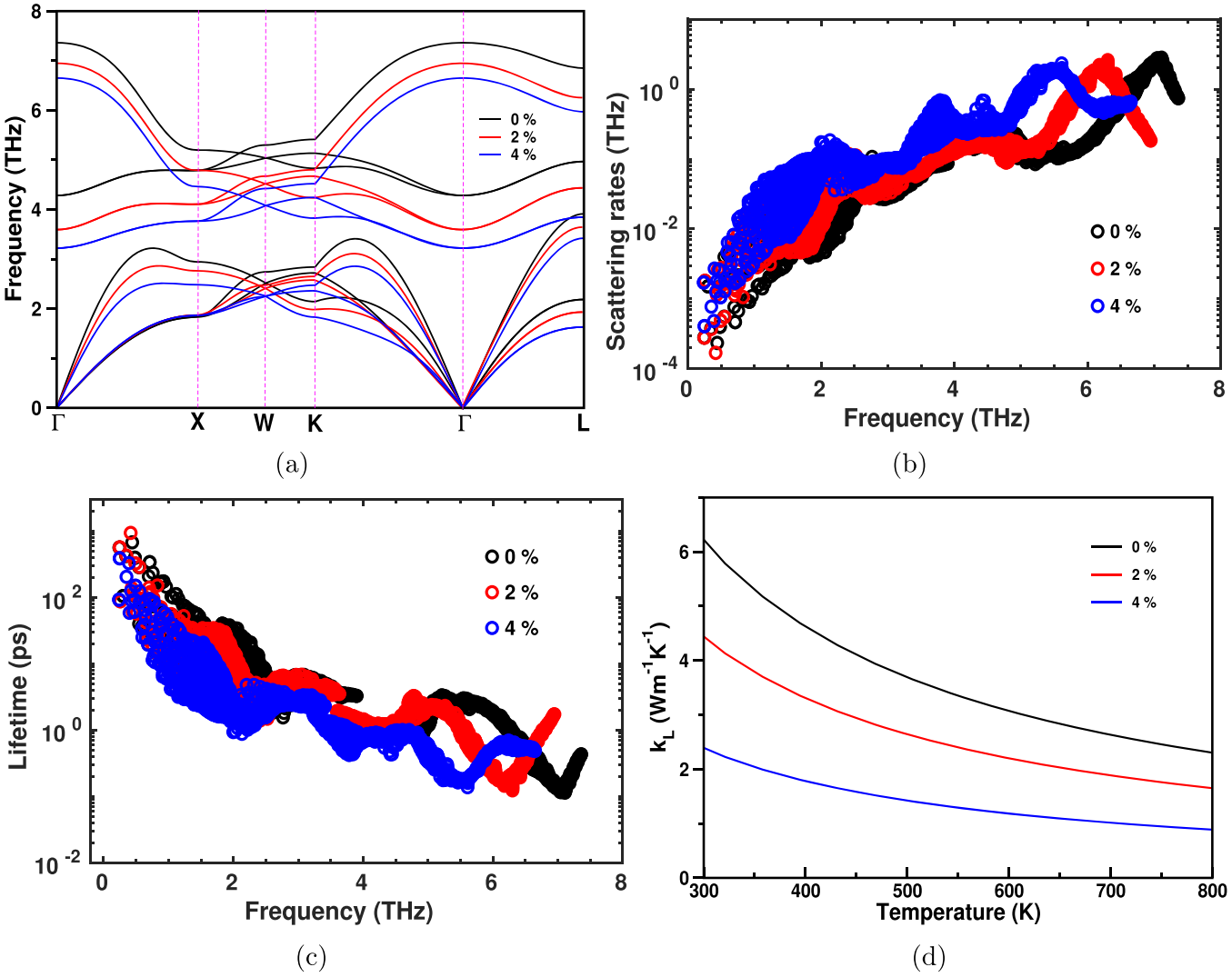

Figure 9. Calculated tensile-strain-dependent (a) phonon dispersion curves, (b) phonon scattering rates, (c) phonon lifetime, and (d) lattice thermal conductivity (k_L) of BaS.

highest and shorter phonon lifetimes in the frequency range of ~1−4 and ~2−4 THz, respectively. This could be a possible reason for the anomalous trend (SrSe > SrO > SrS > SrTe) observed in SrX (X = O, S, Se, and Te) series for k_L. Finally, BaO and BaS have the shortest phonon lifetimes over BaSe and BaTe in turn they have low k_L and this is consistent with the trend BaTe > BaSe > BaS > BaO predicted for k_L in BaX (X = O, S, Se, and Te) compounds.[27]

As shown in Figures S5 and S6, total scattering rates are obtained through summation of absorption, emission, and isotope scattering rates from the three phonon processes for all 16 MX (M = Mg, Ca, Sr, and Ba and X = O, S, Se, and Te) compounds. The absorption scattering rates are largely dominant in the low-frequency region (for instance, below 3 THz for BaO). In the low-frequency region, phonon scattering processes probably occur through conversion of a low-energy phonon to a high-energy phonon with an absorption of a phonon. The contribution of emission scattering rates gradually increase with frequency and are largely dominant in the high-frequency region, where phonon scattering processes probably occur through conversion of a high-energy phonon to a low-energy phonon with an emission of a phonon. Finally, a moderate contribution from isotope scattering rates are observed over the entire frequency range, for instance, BaX (X = O, S, Se, Te) compounds (see Figure S6).

Effect of Tensile Strain on Lattice Thermal Conductivity. Out of 16 MX (M = Mg, Ca, Sr, and Ba and X = O, S, Se, and Te) compounds, three of them (BaO, BaS, and MgTe) were found to have low k_L (<6 W m^{-1} K^{-1}) values over the studied temperature range of 300−800 K. As illustrated in Figure 7, we compared phonon dispersion curves, phonon lifetimes, scattering rates, and k_L values of the BaO, BaS, and MgTe compounds. Phonon softening of both the acoustic and optic modes with a phonon gap because of high mass contrast (see Figure 7a), high scattering rates (see Figure 7b), and short phonon lifetimes (see Figure 7c) is responsible for the low k_L behavior of BaO, BaS, and MgTe compounds. The obtained k_L values follow exactly the decreasing order of phonon lifetimes for these three compounds, which is given as follows: BaS > BaO > MgTe (see Figure 7c, d). On the basis of this trend and observed trends for the rest of the compounds (see Figure 6), we suggest that phonon lifetime (τ) is a dominating factor to determine k_L behavior in isostructural compounds with same crystal symmetry.

We then considered these three BaO, BaS, and MgTe compounds to investigate the effect of tensile strain on lattice

https://doi.org/10.1021/acsaem.1c03310
ACS Appl. Energy Mater. 2022, 5, 882−896

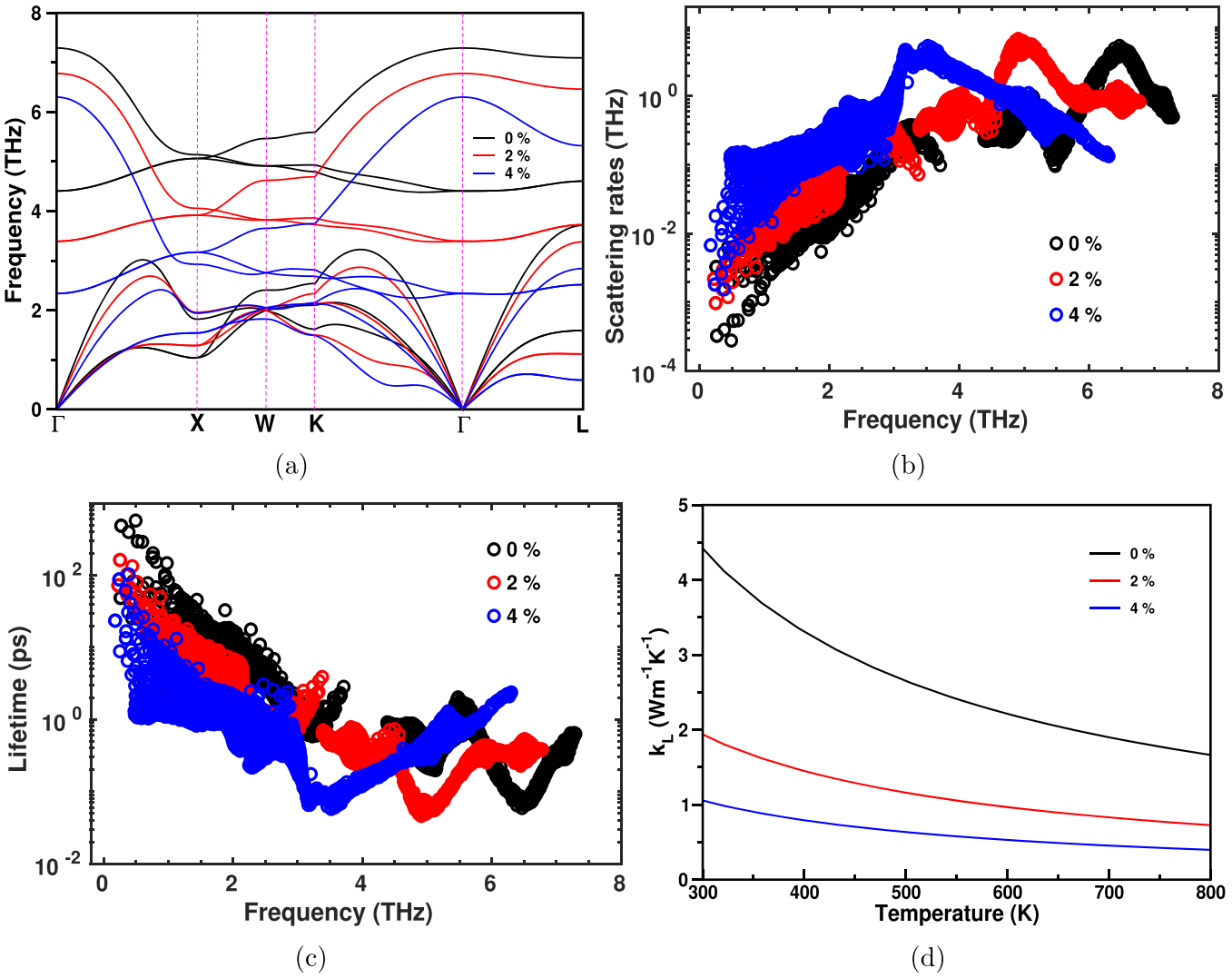

Figure 10. Calculated tensile-strain-dependent (a) phonon dispersion curves, (b) phonon scattering rates, (c) phonon lifetime, and (d) lattice thermal conductivity (k_L) of MgTe.

dynamics and phonon transport. Further, to lower k_L, we applied tensile strain, which is an effective strategy to achieve an (ultra)low k_L in materials. We have systematically increased the obtained equilibrium lattice constant up to 6% but we observed soft phonon modes with tensile strain ≥5% of the equilibrium lattice constant for BaO; therefore, we studied the effect of tensile strain up to 4% for these three compounds. As illustrated in Figures 8a, 9a, and 10a, with increasing strain, the acoustic and TO phonon modes are softened, which increases the coupling strength between the acoustic and TO phonon modes. This eventually increases phonon−phonon scattering rates with increasing strain (see Figure 8b, 9b, and 10b), which causes a reduction in k_L over the studied temperature range. The phonon lifetime decreases (see Figures 8c, 9c, and 10c) significantly because of the high scattering rates for both the acoustic and low-lying TO modes with an increase in tensile strain, which is responsible for further lowering of k_L (see Figures 8d, 9d, and 10d). The obtained k_L values for 4% of tensile strain at 300 K are ∼2.06, ∼2.38, and ∼1.05 W m^{-1} K^{-1} for BaO, BaS, and MgTe, respectively. The ultralow k_L of strained MgTe might be a better candidate for energy conversion applications. From the present and previous studies,[25] one can expect a similar behavior for other MX (M = Mg, Ca, Sr, and Ba and X = O, S, Se, and Te) compounds with an application of tensile strain.

Elastic Constants and Mechanical Properties. To explore the interatomic bonding strength, lattice anharmonicity, and mechanical stability of the investigated compounds, we calculated second-order elastic constants (C_{ij}). Because all the studied MX (M = Mg, Ca, Sr, and Ba and X = O, S, Se, and Te) compounds crystallize in the cubic ($Fm\bar{3}m$) structure, they have three independent elastic constants such as longitudinal (C_{11}), transverse (C_{12}), and shear (C_{44}) due to symmetry constraints ($C_{11} = C_{22} = C_{33}$, $C_{12} = C_{13} = C_{23}$, $C_{44} = C_{55} = C_{66}$, and $C_{ij} = C_{ji}$). The calculated second-order elastic constants are given in Table S4 and are consistent with the available ultrasonic pulse echo[55−57] and Brillouin scattering measurements[58] as well as with previous first-principles calculations.[7,21,54,59−63] The obtained elastic constants satisfy the Born stability criteria[64] indicating the mechanical stability of all these MX (M = Mg, Ca, Sr, and Ba and X = O, S, Se, and Te) compounds.

$$C_{11} - C_{12} > 0,\ C_{11} > 0,\ C_{44} > 0,\ C_{11} + 2C_{12} > 0 \quad (4)$$

We then computed bulk (B) and shear (G) moduli from the calculated elastic constants with Voigt−Reuss−Hill (VRH)

https://doi.org/10.1021/acsaem.1c03310
ACS Appl. Energy Mater. 2022, 5, 882−896

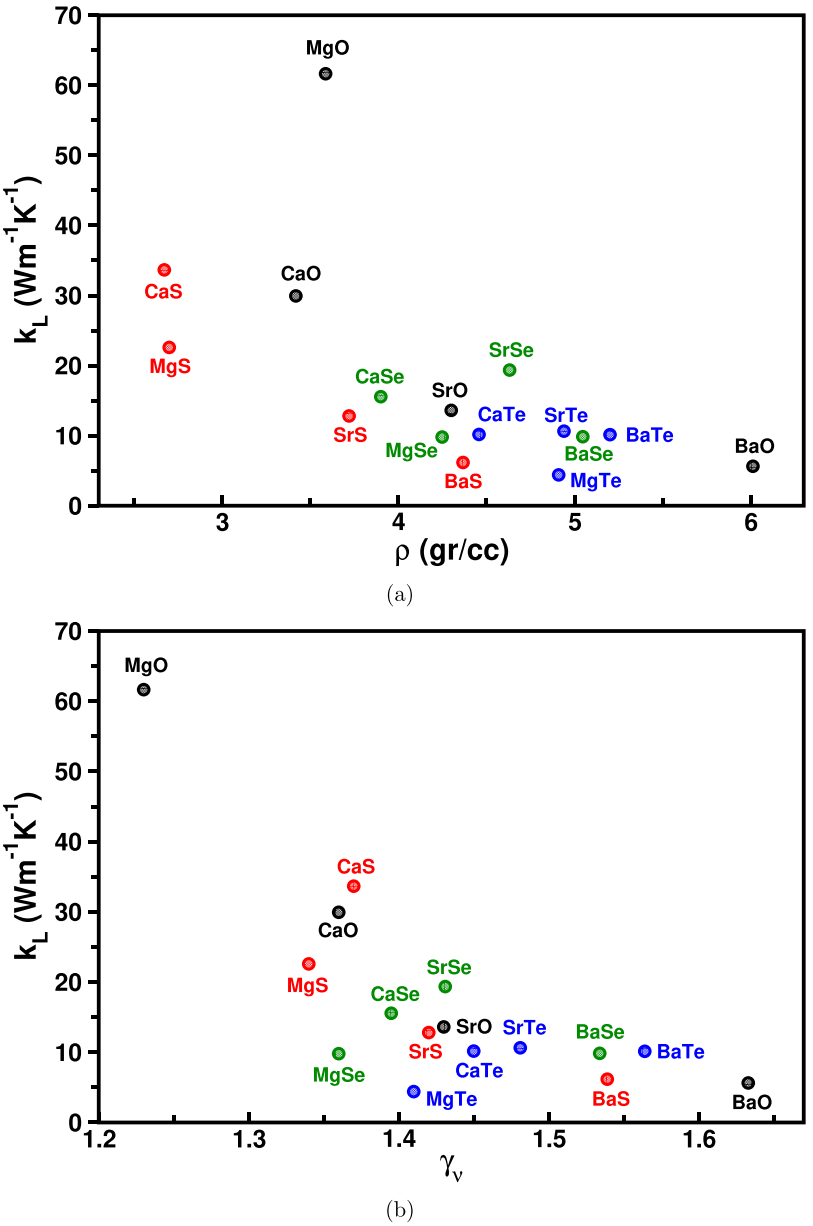

Figure 11. Calculated k_L as a function of (a) density (ρ) and (b) Grüneisen parameter (γ_ν) for 16 MX compounds.

approximation using eqs 5 and 6, respectively. Later, the obtained B and G values are used to calculate Young's modulus (E) using eq 7. Because MgO has the highest E value, it is the stiffest material among the 16 MX (M = Mg, Ca, Sr, and Ba and X = O, S, Se, and Te) compounds.

$$B = \frac{C_{11} + 2C_{12}}{3} \tag{5}$$

$$G = \frac{1}{2}\left[\frac{C_{11} - C_{12} + 3C_{44}}{5} + \frac{5C_{44}(C_{11} - C_{12})}{4C_{44} + 3(C_{11} - C_{12})}\right] \tag{6}$$

$$E = \frac{9BG}{3B + G} \tag{7}$$

The calculated C_{ij} values and E, B, and G moduli decrease from MO to MTe (M = Mg, Ca, Sr, and Ba), which indicates the weak electrostatic/interatomic interactions in the lattice with an increase in atomic size, i.e., from Mg to Ba and O to Te. Therefore, the materials with a higher atomic size can be easily deformed under mechanical stress and thus result in low elastic moduli or soft lattice for systems with higher atomic mass.

$$\nu = \frac{3B - 2G}{2(3B + G)} \tag{8}$$

$$\gamma_\nu = \frac{3}{2}\left(\frac{1 + \nu}{2 - 3\nu}\right) \tag{9}$$

The typical values of Poisson's ratio (ν) are 0.1 and 0.25 for covalent and ionic materials, respectively.[65] The obtained ν values span in the range of 0.18−0.28, which infer a strong ionic contribution in the interatomic bonding for these MX (M = Mg, Ca, Sr, and Ba and X = O, S, Se, and Te) compounds (for instance, see Figure 1 for BaO). MgO (0.18) and BaO (0.28) have the smallest and largest ν values, respectively, among all the 16 MX (M = Mg, Ca, Sr, and Ba and X = O, S,

https://doi.org/10.1021/acsaem.1c03310
ACS Appl. Energy Mater. 2022, 5, 882−896

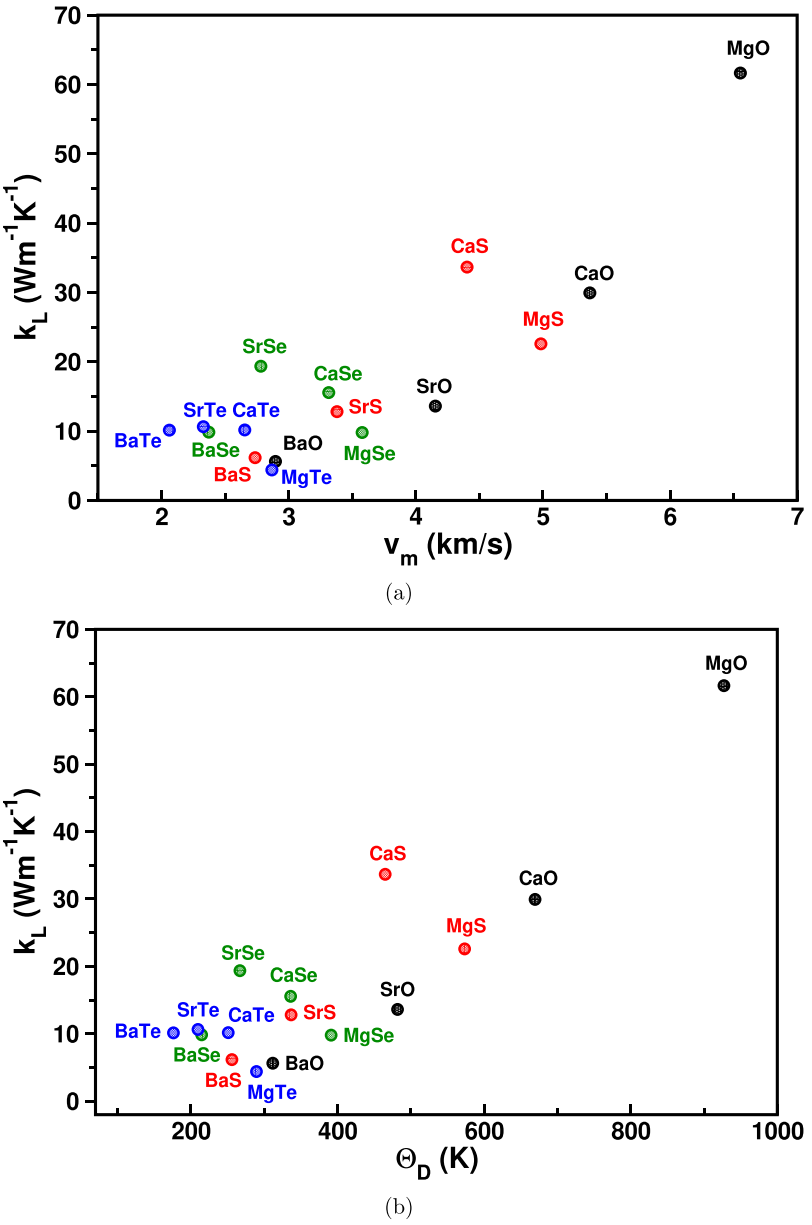

Figure 12. Calculated k_L as a function of (a) average (v_m) sound velocity and (b) Debye temperature (Θ_D) for 16 MX compounds.

Se, and Te) compounds. Further, the ν values are used to calculated the Grüneisen parameter (γ_ν).

The strength of the lattice anharmonicity of a material is represented by the Grüneisen parameter (γ_ω), which is usually obtained from phonons. However, computation of γ_ω involves a series of expensive phonon calculations and repeating them for 16 compounds is computationally demanding. To avoid this, we have used an efficient formula to compute γ_ν using Poisson's ratio (ν).[66] The obtained γ_ν values using eq 9 for materials with rocksalt structure are in excellent agreement with γ_ω as demonstrated in refs67 and 68. Since the 16 materials under investigation crystallize in rocksalt structure, we used eq 9 to compute γ_ν based on the ν values obtained with eq 8. As shown in Figure 11, BaO has the highest γ_ν, which indicates relatively high anharmonicity of BaO over rest of the MX (M = Mg, Ca, and Sr and X = O, S, Se, and Te), BaS, BaSe, and BaTe compounds, which in turn leads to low k_L values. We then calculated sound velocities (v_l, v_t, v_m) and the Debye temperature (Θ_D) using the following relationships:

$$v_l = \sqrt{\frac{B + \frac{4G}{3}}{\rho}} \tag{10}$$

$$v_t = \sqrt{\frac{G}{\rho}} \tag{11}$$

$$v_m = \left[\frac{1}{3}\left(\frac{1}{v_l^3}\right) + \left(\frac{2}{v_t^3}\right)\right]^{-1/3} \tag{12}$$

$$\Theta_D = \frac{h}{k_B}\left[\left(\frac{3N}{4\pi V}\right)\right]^{1/3} v_m \tag{13}$$

Here, ρ, h, k_B, N, and V are the crystal density, Planck constant, Boltzmann constant, and number of atoms and volume of unit cell. The calculated v_l, v_t, v_m, and Θ_D values decrease from MO to MTe (M = Mg, Ca, Sr, and Ba). Figure 12 and Figure S7 show the variation of k_L as a function of Debye temperature

https://doi.org/10.1021/acsaem.1c03310
ACS Appl. Energy Mater. 2022, 5, 882−896

(Θ_D) and average (v_m), longitudinal (v_l), and transverse (v_t) sound velocities for the 16 MX (M = Mg, Ca, Sr, and Ba and X = O, S, Se, and Te) compounds. The same trend is observed for all these four properties v_l, v_t, v_m, and Θ_D. According to the Slack theory, low Θ_D values are indicative of low k_L values in materials. In fact, the presence of LLO phonons results in a softening of the acoustic phonon modes, which yields low group velocities and frequencies for acoustic phonons and thus results in low Θ_D. However, BaO, BaS, and MgTe compounds have low k_L values despite their higher v_l, v_t, v_m, and Θ_D over other MTe (M = Ca, Sr, Ba), BaSe, and SrSe compounds. Moreover, the calculated phonon group velocities for BaX (X = O, S, and Se) compounds (see Figure S8) also follow their atomic mass trend consistent with sound velocities. Overall, the results of present study strongly suggest that high mass contrast and phonon lifetimes are the dominant factors that are responsible for the observed anomalous trends in MX (M = Mg, Ca, Sr, and Ba and X = O, S, Se, and Te) compounds.

CONCLUSIONS

In summary, we have systematically investigated lattice dynamics, phonon transport, and mechanical properties of 16 binary compounds with rocksalt-type structure. We predicted anomalous trends for k_L in CaX (CaS > CaO > CaSe > CaTe), SrX (SrSe > SrO > SrS > SrTe), and BaX (BaTe > BaSe > BaS > BaO) series of compounds. In particular, we observed an opposite trend for k_L in the BaX (X = O, S, Se, and Te) series, which is in contrast to the expected trend from their atomic mass. However, the above trends are slightly altered for SrX (X = O, S, and Se) and BaX (X = O, S, Se, and Te) compounds, when k_L is computed at the experimental lattice constant because of the sensitivity of k_L toward the lattice constant. We propose few observations from this study to design (ultra)low k_L materials, which are as follows: (1) design a material with a combination of heavy and light elements to have high mass contrast, which produces an acoustic-optic phonon gap, (2) phonon softening of transverse acoustic (TA) modes due to heavy atomic mass element; (3) constituent elements in a material with a high electronegativity difference produce a large LO-TO splitting, resulting in LLO (TO) phonon modes, which might fall into the acoustic mode region, and they are responsible for the softening of acoustic phonon modes or enhancing the overlap between the LLO and longitudinal acoustic (LA) phonon modes, thereby increasing scattering rates thus resulting in shorter phonon lifetimes; and (4) selection of a material with a relatively high density (ρ). The application of tensile strain further reduces k_L in BaO, BaS, and MgTe through phonon softening, which increases scattering rates, thereby lowering phonon lifetimes. Overall, the present study provides insights to achieve (ultra)low k_L materials through phonon engineering in simple crystal systems, which is essential for the development of sustainable energy conversion devices for future energy applications.

ASSOCIATED CONTENT

Supporting Information

The Supporting Information is available free of charge at https://pubs.acs.org/doi/10.1021/acsaem.1c03310.

Temperature-dependent lattice thermal conductivity (Figures S1 and S2), lattice transport properties of CaO and CaS (Figure S3), frequency-dependent mean free paths (Figure S4) and scattering rates (Figures S5 and S6), lattice thermal conductivity as a function of sound velocities (Figure S7), frequency-dependent phonon group velocities for BaO, BaS, and BaSe (Figure S8); ground-state structural properties (Table S1), Born effective charges, LO and TO phonon modes (Table S2 and S3), elastic constants (Table S4), and polycrystalline elastic properties (Table S5) (PDF)

AUTHOR INFORMATION

Corresponding Authors

S. C. Rakesh Roshan − *Rajiv Gandhi University of Knowledge Technologies, Basar 504107 Telangana, India; Department of Physics, National Institute of Technology-Warangal, Warangal 506 004 Telangana, India*; Email: roshan@rgukt.ac.in

N. Yedukondalu − *Department of Geosciences, Center for Materials by Design, and Institute for Advanced Computational Science, State University of New York, Stony Brook, New York 11794-2100, United States*; orcid.org/0000-0002-7650-7567; Email: nykondalu@gmail.com

Authors

Rajmohan Muthaiah − *School of Aerospace and Mechanical Engineering, University of Oklahoma, Norman, Oklahoma 73019, United States*

Kunduru Lavanya − *Jawaharlal Nehru Technological University (JNTU), Hyderabad 500085 Telangana, India; Telangana Social Welfare Residential Degree College for Women (TSWRDC-W), Nizamabad 503 002 Telangana, India*

Pazhedath Anees − *Materials Physics Division, Indira Gandhi Centre for Atomic Research, Kalpakkam 603102 Tamil Nadu, India*; orcid.org/0000-0003-1719-9741

Rajaboina Rakesh Kumar − *Department of Physics, Energy Materials and Devices Lab, National Institute of Technology-Warangal, Warangal 506004 Telangana, India*; orcid.org/0000-0003-4023-9051

Tumu Venkatappa Rao − *Department of Physics, Energy Materials and Devices Lab, National Institute of Technology-Warangal, Warangal 506004 Telangana, India*

Lars Ehm − *Department of Geosciences, Center for Materials by Design, and Institute for Advanced Computational Science, State University of New York, Stony Brook, New York 11794-2100, United States*

John B. Parise − *Department of Geosciences, Center for Materials by Design, and Institute for Advanced Computational Science, State University of New York, Stony Brook, New York 11794-2100, United States*

Complete contact information is available at: https://pubs.acs.org/10.1021/acsaem.1c03310

Author Contributions

S.C.R.R. and N.Y.K. contributed equally to the manuscript.

Notes

The authors declare no competing financial interest.

ACKNOWLEDGMENTS

S.C.R.R. thanks RGUKT Basar for providing computational facilities. N.Y.K. thanks Prof. Olle Hellman, Linköping University, Sweden, for his valuable suggestions and discussions. N.Y.K. also thank the Science and Engineering Research Board and the Indo-US Scientific Technology Forum

for providing financial support through a SERB Indo-US postdoctoral fellowship and Stony Brook Research Computing and Cyberinfrastructure, and the Institute for Advanced Computational Science at Stony Brook University for access to the high-performance SeaWulf computing system, which was made possible by a $1.4M National Science Foundation grant (1531492).

REFERENCES

(1) Ding, J.; Lanigan-Atkins, T.; Calderón-Cueva, M.; Banerjee, A.; Abernathy, D. L.; Said, A.; Zevalkink, A.; Delaire, O. Soft anharmonic phonons and ultralow thermal conductivity in $Mg_3(Sb, Bi)_2$ thermoelectrics. *Science Advances* **2021**, *7*, No. eabg1449.
(2) Dutta, M.; Sarkar, D.; Biswas, K. Intrinsically ultralow thermal conductive inorganic solids for high thermoelectric performance. *Chem. Commun.* **2021**, *57*, 4751−4767.
(3) Liu, B.; Liu, Y.; Zhu, C.; Xiang, H.; Chen, H.; Sun, L.; Gao, Y.; Zhou, Y. Advances on strategies for searching for next generation thermal barrier coating materials. *Journal of Materials Science & Technology* **2019**, *35*, 833−851.
(4) Bsaibess, E.; Delorme, F.; Monot-Laffez, I.; Giovannelli, F. Ultralow thermal conductivity in scheelite and A-deficient scheelite ceramics. *Scripta Materialia* **2021**, *201*, 113950.
(5) Rajput, K.; Roy, D. R. h-CaS and h-CaSe nanosheets in CaX (X = O, S, Se and Te) series: promising thermoelectric materials under DFT investigation. *Applied Nanoscience* **2019**, *9*, 1845−1856.
(6) Rajput, K.; Roy, D. R. Structure, stability, electronic and thermoelectric properties of strontium chalcogenides. *Physica E: Low-dimensional Systems and Nanostructures* **2020**, *119*, 113965.
(7) Kumar, P.; Rajput, K.; Roy, D. R. Structural, electronic, vibrational, mechanical and thermoelectric properties of 2D and bulk BaX (X = O, S, Se and Te) series under DFT and BTE framework. *Physica E: Low-dimensional Systems and Nanostructures* **2021**, *127*, 114523.
(8) Zheng, H.; Li, X.-B.; Chen, N.-K.; Xie, S.-Y.; Tian, W. Q.; Chen, Y.; Xia, H.; Zhang, S. B.; Sun, H.-B. Monolayer II-VI semiconductors: A first-principles prediction. *Phys. Rev. B* **2015**, *92*, 115307.
(9) Biswas, K.; He, J.; Wang, G.; Lo, S.-H.; Uher, C.; Dravid, V. P.; Kanatzidis, M. G. High thermoelectric figure of merit in nanostructured p-type PbTe−MTe (M = Ca, Ba). *Energy Environ. Sci.* **2011**, *4*, 4675−4684.
(10) Al Rahal Al Orabi, R.; Mecholsky, N. A.; Hwang, J.; Kim, W.; Rhyee, J.-S.; Wee, D.; Fornari, M. Band Degeneracy, Low Thermal Conductivity, and High Thermoelectric Figure of Merit in SnTe−CaTe Alloys. *Chem. Mater.* **2016**, *28*, 376−384.
(11) Tan, G.; Shi, F.; Hao, S.; Zhao, L.-D.; Chi, H.; Zhang, X.; Uher, C.; Wolverton, C.; Dravid, V. P.; Kanatzidis, M. G. Non-equilibrium processing leads to record high thermoelectric figure of merit in PbTe-SrTe. *Nat. Commun.* **2016**, *7*, 12167.
(12) Kim, Y.-J.; Zhao, L.-D.; Kanatzidis, M. G.; Seidman, D. N. Analysis of Nanoprecipitates in a Na-Doped PbTe−SrTe Thermoelectric Material with a High Figure of Merit. *ACS Appl. Mater. Interfaces* **2017**, *9*, 21791−21797.
(13) Lo, S.-H.; He, J.; Biswas, K.; Kanatzidis, M. G.; Dravid, V. P. Phonon Scattering and Thermal Conductivity in p-Type Nanostructured PbTe-BaTe Bulk Thermoelectric Materials. *Adv. Funct. Mater.* **2012**, *22*, 5175−5184.
(14) Fan, T.; Oganov, A. R. Discovery of high performance thermoelectric chalcogenides through first-principles high-throughput screening. *J. Mater. Chem. C* **2021**, *9*, 13226−13235.
(15) Abdus Salam, M. M. Theoretical study of CaO, CaS and CaSe via first-principles calculations. *Results in Physics* **2018**, *10*, 934−945.
(16) Hao, A. M.; Yang, X. C.; Gao, Z. M.; Liu, X.; Zhu, Y.; Liu, R. P. First-principles investigations on structural and elastic properties of CaX (X = S, Se and Te) under high pressure. *High Pressure Research* **2010**, *30*, 310−317.
(17) Bayrakci, M.; Colakoglu, K.; Deligoz, E.; Ciftci, Y. O. A first-principle study of the structural and lattice dynamical properties of CaX (X = S, Se, and Te). *High Pressure Research* **2009**, *29*, 187−203.
(18) Ugur, S. Theoretical study of the phonon properties of SrS. *Materials Science and Engineering: B* **2009**, *162*, 116−119.
(19) Rakesh Roshan, S.; Kunduru, L.; Yedukondalu, N.; Sainath, M. Structure and Lattice Dynamics of Calcium Chalcogenides under High Pressure. *Materials Today: Proceedings* **2018**, *5*, 18874−18878.
(20) Zhang, X.-D.; Li, Z.-J.; Shi, G.-M. Lattice Dynamics Study of Magnesium Chalcogenides. *Commun. Theor. Phys.* **2012**, *57*, 295−300.
(21) Varshney, D.; Jain, S.; Shriya, S.; Khenata, R. High-pressure and temperature-induced structural, elastic, and thermodynamical properties of strontium chalcogenides. *Journal of Theoretical and Applied Physics* **2016**, *10*, 163−193.
(22) Musari, A. A.; Orukombo, S. A. Theoretical study of phonon dispersion, elastic, mechanical and thermodynamic properties of barium chalcogenides. *International Journal of Modern Physics B* **2018**, *32*, 1850092.
(23) Muthaiah, R.; Garg, J. Thermal conductivity of magnesium selenide MgSe−A first principles study. *Comput. Mater. Sci.* **2021**, *198*, 110679.
(24) Muthaiah, R.; Garg, J. Thermal conductivity of magnesium telluride MgTe - A first principles study. *Solid State Commun.* **2021**, *337*, 114414.
(25) Yang, Z.; Yuan, K.; Meng, J.; Zhang, X.; Tang, D.; Hu, M. Why thermal conductivity of CaO is lower than that of CaS: a study from the perspective of phonon splitting of optical mode. *Nanotechnology* **2021**, *32*, 025709.
(26) Xia, Y.; Hodges, J. M.; Kanatzidis, M. G.; Chan, M. K. Y. Lattice thermal transport in group II-alloyed PbTe. *Appl. Phys. Lett.* **2018**, *112*, 181906.
(27) Seko, A.; Togo, A.; Hayashi, H.; Tsuda, K.; Chaput, L.; Tanaka, I. Prediction of Low-Thermal-Conductivity Compounds with First-Principles Anharmonic Lattice-Dynamics Calculations and Bayesian Optimization. *Phys. Rev. Lett.* **2015**, *115*, 205901.
(28) Kresse, G.; Furthmüller, J. Efficient iterative schemes for ab initio total-energy calculations using a plane-wave basis set. *Phys. Rev. B* **1996**, *54*, 11169−11186.
(29) Hellman, O.; Abrikosov, I. A.; Simak, S. I. Lattice dynamics of anharmonic solids from first principles. *Phys. Rev. B* **2011**, *84*, 180301.
(30) Hellman, O.; Abrikosov, I. A. Temperature-dependent effective third-order interatomic force constants from first principles. *Phys. Rev. B* **2013**, *88*, 144301.
(31) Hellman, O.; Steneteg, P.; Abrikosov, I. A.; Simak, S. I. Temperature dependent effective potential method for accurate free energy calculations of solids. *Phys. Rev. B* **2013**, *87*, 104111.
(32) Luo, H.; Greene, R. G.; Ghandehari, K.; Li, T.; Ruoff, A. L. Structural phase transformations and the equations of state of calcium chalcogenides at high pressure. *Phys. Rev. B* **1994**, *50*, 16232−16237.
(33) Zimmer, H. G.; Winzen, H.; Syassen, K. High-pressure phase transitions in CaTe and SrTe. *Phys. Rev. B* **1985**, *32*, 4066−4070.
(34) Yamaoka, S.; Shimomura, O.; Nakazawa, H.; Fukunaga, O. Pressure-induced phase transformation in BaS. *Solid State Commun.* **1980**, *33*, 87−89.
(35) Syassen, K.; Christensen, N. E.; Winzen, H.; Fischer, K.; Evers, J. Optical response and band-structure calculations of alkaline-earth tellurides under pressure. *Phys. Rev. B* **1987**, *35*, 4052−4059.
(36) Wyckoff, R. W. G. *Crystal Structures*, 2nd ed.; Interscience Publishers: New York, 1963; Vol. *1*.
(37) Liu, L.-g.; Bassett, W. A. Effect of pressure on the crystal structure and the lattice parameters of BaO. *J. Geophys. Res.* **1972**, *77*, 4934−4937.
(38) Yamaoka, S.; Shimomura, O.; Nakazawa, H.; Fukunaga, O. Pressure-induced phase transformation in BaS. *Solid State Commun.* **1980**, *33*, 87−89.
(39) Waag, A.; Heinke, H.; Scholl, S.; Becker, C.; Landwehr, G. Growth of MgTe and $Cd_{1-x}Mg_xTe$ thin films by molecular beam epitaxy. *J. Cryst. Growth* **1993**, *131*, 607−611.

https://doi.org/10.1021/acsaem.1c03310
ACS Appl. Energy Mater. 2022, 5, 882−896

(40) Li, T.; Luo, H.; Greene, R. G.; Ruoff, A. L.; Trail, S. S.; DiSalvo, F. J., Jr. High Pressure Phase of MgTe: Stable Structure at STP? *Phys. Rev. Lett.* **1995**, *74*, 5232−5235.
(41) Tairi, L.; Touam, S.; Boumaza, A.; Boukhtouta, M.; Meradji, H.; Ghemid, S.; Omran, S. B.; Hassan, F. E. H.; Khenata, R. Phase stability and electronic behavior of MgS, MgSe and MgTe compounds. *Phase Transitions* **2017**, *90*, 929−941.
(42) Duman, S.; Bağcı, S.; Tütüncü, H. M.; Srivastava, G. P. First-principles studies of ground-state and dynamical properties of MgS, MgSe, and MgTe in the rocksalt, zinc blende, wurtzite, and nickel arsenide phases. *Phys. Rev. B* **2006**, *73*, 205201.
(43) Chakrabarti, A. Role of NiAs phase in pressure-induced structural phase transitions in IIA-VI chalcogenides. *Phys. Rev. B* **2000**, *62*, 1806−1814.
(44) Van Camp, P. E.; Van Doren, V. E.; Martins, J. L. High-pressure phases of magnesium selenide and magnesium telluride. *Phys. Rev. B* **1997**, *55*, 775−779.
(45) Fei, Y. Effects of temperature and composition on the bulk modulus of (Mg,Fe)O. *Am. Mineral.* **1999**, *84*, 272−276.
(46) Richet, P.; Mao, H.-K.; Bell, P. M. Static compression and equation of state of CaO to 1.35 Mbar. *Journal of Geophysical Research: Solid Earth* **1988**, *93*, 15279−15288.
(47) Pandey, R.; Sutjianto, A. Study of structural phase transition in MgSe. *Solid State Commun.* **1994**, *91*, 269−271.
(48) Baltache, H.; Khenata, R.; Sahnoun, M.; Driz, M.; Abbar, B.; Bouhafs, B. Full potential calculation of structural, electronic and elastic properties of alkaline earth oxides MgO, CaO and SrO. *Physica B: Condensed Matter* **2004**, *344*, 334−342.
(49) Mir, S. H.; Jha, P. C.; Dabhi, S.; Jha, P. K. Ab initio study of phase stability, lattice dynamics and thermodynamic properties of magnesium chalcogenides. *Mater. Chem. Phys.* **2016**, *175*, 54−61.
(50) Kürkçü, C. An Ab-initio Study of Structural and Electronic Properties of CaTe under High Pressure. *Russian Journal of Physical Chemistry A* **2019**, *93*, 2226−2232.
(51) Khenata, R.; Baltache, H.; Rérat, M.; Driz, M.; Sahnoun, M.; Bouhafs, B.; Abbar, B. First-principle study of structural, electronic and elastic properties of SrS, SrSe and SrTe under pressure. *Physica B: Condensed Matter* **2003**, *339*, 208−215.
(52) Toberer, E. S.; Zevalkink, A.; Snyder, G. J. Phonon engineering through crystal chemistry. *J. Mater. Chem.* **2011**, *21*, 15843−15852.
(53) Slack, G. Nonmetallic crystals with high thermal conductivity. *J. Phys. Chem. Solids* **1973**, *34*, 321−335.
(54) Ren, Y. First principles study of electronic, phonon and elastic properties of rock-salt-phase MTe (M = Mg, Ca, Sr, Ba). *Computational Condensed Matter* **2017**, *11*, 69−76.
(55) Son, P.; Bartels, R. CaO and SrO single crystal elastic constants and their pressure derivatives. *J. Phys. Chem. Solids* **1972**, *33*, 819−828.
(56) Anderson, O. L.; Andreatch, P. Pressure Derivatives of Elastic Constants of Single-Crystal MgO at 23° and −195.8°C. *J. Am. Ceram. Soc.* **1966**, *49*, 404−409.
(57) Vetter, V.; Bartels, R. BaO single crystal elastic constants and their temperature dependence. *J. Phys. Chem. Solids* **1973**, *34*, 1448−1449.
(58) Sinogeikin, S. V.; Bass, J. D. Single-crystal elasticity of MgO at high pressure. *Phys. Rev. B* **1999**, *59*, R14141−R14144.
(59) Cinthia, A. J.; Priyanga, G. S.; Rajeswarapalanichamy, R.; Iyakutti, K. Structural, electronic and mechanical properties of alkaline earth metal oxides MO (M = Be, Mg, Ca, Sr, Ba). *J. Phys. Chem. Solids* **2015**, *79*, 23−42.
(60) Abdus Salam, M. M. First principles study of structural, elastic and electronic structural properties of strontium chalcogenides. *Chinese Journal of Physics* **2019**, *57*, 418−434.
(61) Maizi, R.; Boudjahem, A.-G.; Boulbazine, M. First-Principles Investigations on Structural, Elastic, and Thermodynamic Properties of CaX (X = S, Se, and Te) under Pressure. *Russian Journal of Physical Chemistry A* **2019**, *93*, 2726−2734.
(62) Wu, H.; Chen, Y.; Deng, C.; Han, X.; Yin, P. Electronic, elastic and dynamical properties of MgSe under pressure: rocksalt and iron silicide phase. *Philos. Mag.* **2015**, *95*, 2240−2256.
(63) Guo, Y.; Xia, D.; Liu, Q.; Zhao, X.; Li, J. Phase transition of CaTe induced by high-pressure: Structural and elastic DFT study of five structures. *Solid State Commun.* **2021**, *340*, 114488.
(64) Born, M. On the stability of crystal lattices. I. *Mathematical Proceedings of the Cambridge Philosophical Society* **1940**, *36*, 160−172.
(65) Haines, J.; Léger, J.; Bocquillon, G. Synthesis and Design of Superhard Materials. *Annu. Rev. Mater. Res.* **2001**, *31*, 1−23.
(66) Sanditov, D. S.; Belomestnykh, V. N. Relation between the parameters of the elasticity theory and averaged bulk modulus of solids. *Technical Physics* **2011**, *56*, 1619−1623.
(67) Xiao, Y.; Chang, C.; Pei, Y.; Wu, D.; Peng, K.; Zhou, X.; Gong, S.; He, J.; Zhang, Y.; Zeng, Z.; et al. Origin of low thermal conductivity in SnSe. *Phys. Rev. B* **2016**, *94*, 125203.
(68) Jia, T.; Chen, G.; Zhang, Y. Lattice thermal conductivity evaluated using elastic properties. *Phys. Rev. B* **2017**, *95*, 155206.
(69) II-VI and I-VII Compounds. In *Semimagnetic Compounds*; Madelung, O., Rössler, U., Schulz, M., Eds.; Springer-Verlag, 1999.
(70) Xia, Y.; Hegde, V. I.; Pal, K.; Hua, X.; Gaines, D.; Patel, S.; He, J.; Aykol, M.; Wolverton, C. High-Throughput Study of Lattice Thermal Conductivity in Binary Rocksalt and Zinc Blende Compounds Including Higher-Order Anharmonicity. *Phys. Rev. X* **2020**, *10*, 041029.

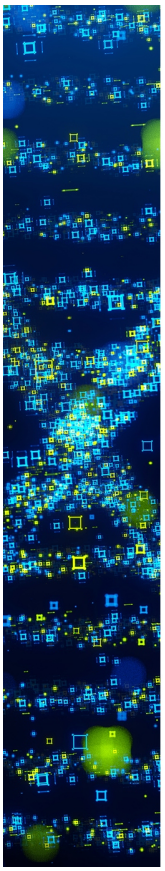
CAS BIOFINDER DISCOVERY PLATFORM™
STOP DIGGING THROUGH DATA —START MAKING DISCOVERIES
CAS BioFinder helps you find the right biological insights in seconds
Start your search
CAS
A division of the American Chemical Society

https://doi.org/10.1021/acsaem.1c03310
ACS Appl. Energy Mater. 2022, 5, 882−896